Available online at www.sciencedirect.com
SCIENCE DIRECT®
Journal of Computational Physics 188 (2003) 333–347
JOURNAL OF COMPUTATIONAL PHYSICS
www.elsevier.com/locate/jcp

High-resolution Burnett simulations of micro Couette flow and heat transfer

Duncan A. Lockerby, Jason M. Reese *

Department of Mechanical Engineering, King's College London, London WC2R 2LS, UK

Received 28 August 2002; received in revised form 27 February 2003; accepted 5 March 2003

Abstract

A high-order continuum model for micro-scale flows is investigated. The Burnett equations are applied to the steady-state micro Couette flow of a Maxwellian monatomic gas. Solutions to these equations are shown to be stable for all Knudsen numbers (Kn) up to the limit of the equations' validity ($Kn \to 1$). The reason why previous researchers have failed to obtain solutions to this problem for Kn much greater than 0.1 is explained. A procedure is proposed to overcome these difficulties, and its application successfully demonstrated. Results are obtained on high-resolution numerical grids and show good agreement with data obtained from direct simulation methods. A reduced-order procedure is also described for calculating the implicitly defined first-order slip boundary conditions prior to the solution of the full equations. This method can be used to generate accurate initial guesses for an iterative solution. The comparative utility of second-order boundary conditions is explored and alternatives discussed.

Keywords: Microfluidics; Burnett equations; Micro Couette flow; Second-order continuum methods; Rarefied flows; Microelectromechanical systems; MEMS

1. Introduction

Understanding the dynamics of gas flows in and around micron-scale geometries (*microfluidics*) is important for the design of certain microelectromechanical systems (MEMS) e.g., microchromatographs, microactuators for aerodynamic flow control, microturbines and pumps, etc. [4]. However, the Navier–Stokes equations with non-slip boundary conditions do not apply because they can only describe flows that are close to local equilibrium which, in general, gas flows in MEMS rarely are [3]. This is because the mean free path of the gas molecules at typical MEMS operating temperatures and pressures approaches the length scale of the microdevice itself, so there are not enough collisions to equilibrate heat and momentum at every point in the flow. The critical parameter in this problem is the well-known Knudsen number,

* Corresponding author. Tel.: +44-20-7847-2322; fax: +44-20-7848-2932.
E-mail addresses: duncan.lockerby@kcl.ac.uk (D.A. Lockerby), jason.reese@kcl.ac.uk (J.M. Reese).

0021-9991/03/$ - see front matter
doi:10.1016/S0021-9991(03)00162-1

$Kn = \lambda/L$, where λ is the mean free path of the molecules and L is a distinctive spatial dimension of the flow. The Navier–Stokes equations with non-slip wall conditions are only appropriate when $Kn < 0.001$ [3]. But gas flows in MEMS are often in the "continuum transition" regime, i.e. $0.001 < Kn < 10$. In this case the gas acts neither as a continuous fluid ($Kn < 0.001$) nor as a free molecular flow in which molecular collisions are unimportant.

Although the common solution to modelling flows in the continuum transition regime is to use a molecular dynamics or Monte Carlo approach, these can be extremely computationally intensive, especially for complex flow geometries. In a previous paper [9], one of the authors and his colleagues showed that certain macro-scale continuum transition flows can be described by extended governing equations, with continuum-type expressions for the viscous stress and heat flux terms derived from a *Kn*-series solution to the Boltzmann equation [2]. To first order, this series solution technique yields the Navier–Stokes equations; to second order, the so-called Burnett equations. Differing physical interpretations and approaches to the series solution technique for the Boltzmann equation have also, in recent years, led to competing sets of second-order equations, including the BGK-Burnett [1], Grad [2], Eu [7] and Woods [10] equations. Although the complexity, nonlinearity and numerical instability associated with all these equations has impeded research into their predictive capacity, it is generally recognised that this class of equations should be the most appropriate for modelling flows in the continuum transition regime, whether at the macro- or micro-scale. In addition, provided numerically stable and unique solutions can be found, the numerical effort involved in their solution would be orders of magnitude less than molecular dynamics or Monte Carlo techniques, and comparable to current Computational Fluid Dynamics. This extended-continuum approach could form the basis for a new methodology for high-*Kn* flows in MEMS, and be a practical and accurate approach to investigating new fluid flow and heat transfer phenomena at micron scales.

This paper describes such an investigation, using the classical Burnett equations to describe steady, compressible Couette flow of a Maxwellian monatomic gas at the micro-scale. Following a general introduction to the equations, the numerical stability of the Burnett equations applied to micro Couette flow is examined. The reason why previous researchers have been unable to obtain solutions to these equations, over a wide range of *Kn*, is demonstrated and a new solution procedure proposed. The new technique is then applied to plane micro Couette flow in one dimension and, in the absence of experimental data, results obtained are compared with data from previous Monte Carlo simulations. The accuracy and effectiveness of using second-order transport equations for investigating flows at the micro-scale are then assessed.

2. The Burnett equations

Although, as mentioned in Section 1, there are a number of sets of governing equations available, all to second-order in *Kn*, no consensus has yet emerged as to which set is the most physically consistent. Therefore, the equations adopted in this paper are the classical and accepted form of the Burnett equations. Apart from being the most well-established, they have notorious problems with both ill-posedness [5] and the related time-dependent instability [12]. Recently, there has also been some doubt raised about the physicality of certain terms within the equations [10]. However, if solutions can be obtained using the Burnett equations, it is likely that a similar methodology will also be successful for the other sets of available equations.

In this paper, the gas is assumed to be Maxwellian molecular and monatomic, and the flows steady and one-dimensional. These assumptions significantly simplify the Burnett equations, though the findings are not necessarily limited to this idealised case.

At each point in space and time, the state of a monatomic ideal gas flow is determined by its velocity $\mathbf{v}$, temperature T and density ρ. We assume the pressure, p, obeys the perfect gas law

$$p = \rho R T, \tag{1}$$

where $R = k_b/m$ is the gas constant, k_b is the Boltzmann constant and m is the molecular mass. Specific heats at constant volume and pressure are denoted c_v and c_p, respectively. A monatomic ideal gas is characterized by the relations

$$c_v = \frac{3}{2}R \quad \text{and} \quad c_p = \frac{5}{2}R \tag{2}$$

such that the isentropic constant γ, defined as the ratio of c_p to c_v, is equal to 5/3. The speed of sound c is given in the medium by the simple relation

$$c^2 = \gamma \frac{p}{\rho}. \tag{3}$$

The conservation equations for momentum and energy include a viscous stress tensor $\mathbf{\Pi}$ and a heat flux vector $\mathbf{Q}$. These transport terms may be obtained through the classical Chapman–Enskog expansion in Knudsen number of the Boltzmann equation [2]:

$$\mathbf{\Pi} = \mathbf{\Pi}^{(0)} + \mathbf{\Pi}^{(1)} + \mathbf{\Pi}^{(2)} + \cdots, \tag{4a}$$

$$\mathbf{Q} = \mathbf{Q}^{(0)} + \mathbf{Q}^{(1)} + \mathbf{Q}^{(2)} + \cdots \tag{4b}$$

At zeroth-order, this procedure gives

$$\mathbf{\Pi}^{(0)} = p\mathbf{1}, \tag{5a}$$

$$\mathbf{Q}^{(0)} = \mathbf{0}. \tag{5b}$$

When these fluxes are used in the conservation equations, the governing equations are termed the Euler equations.

The next approximation gives:

$$\mathbf{\Pi}^{(1)} = -2\mu\mathring{\mathbf{e}}, \tag{6a}$$

$$\mathbf{Q}^{(1)} = -\kappa\nabla T, \tag{6b}$$

where, in tensor notation, $\mathring{\mathbf{e}} \equiv \mathbf{e} - (1/3)\,\mathrm{tr}(\mathbf{e})\mathbf{1}$ and $\mathbf{e} = (1/2)(\nabla\mathbf{v} + \nabla\mathbf{v}^{\mathrm{t}})$, and μ and κ are, respectively, the viscosity and the heat conductivity of the gas. For a monatomic gas modeled by point centres of force, the kinetic theory leads to a viscosity proportional to T^s and the Prandtl number $\mathrm{Pr} = \mu c_p/\kappa$ is a constant equal to 2/3. For a Maxwellian molecular gas, the temperature exponent s is simply 1. The conservation equations together with the fluxes (6a), (6b) define the Navier–Stokes equations.

At second-order in Kn, the series solution technique leads to the accepted form of the Burnett expressions for viscous stress and heat flux [2]:

$$\mathbf{\Pi}^{(2)} = \frac{\mu^2}{p}\left[\tilde{\omega}_1\nabla\cdot\mathbf{v}\mathring{\mathbf{e}}. + \tilde{\omega}_2\left(D\mathring{\mathbf{e}} - 2\overline{\nabla\mathbf{v}\cdot\mathring{\mathbf{e}}}^{\circ}\right) + \tilde{\omega}_3 R\overline{\nabla\nabla T}^{\circ} + \frac{\tilde{\omega}_4}{\rho T}\overline{\nabla p\nabla T}^{\circ} + \tilde{\omega}_5\frac{R}{T}\overline{\nabla T\nabla T}^{\circ} + \tilde{\omega}_6\overline{\mathring{\mathbf{e}}\cdot\mathring{\mathbf{e}}}^{\circ}\right], \tag{7a}$$

$$\mathbf{Q}^{(2)} = R\frac{\mu^2}{p}\left[\theta_1\nabla\cdot\mathbf{v}\nabla T + \theta_2\left(D\nabla T - \nabla\mathbf{v}\cdot\nabla T\right) + \theta_3\frac{T}{p}\nabla p\cdot\mathring{\mathbf{e}} + \theta_4 T\nabla\cdot\mathring{\mathbf{e}} + 3\theta_5\nabla T\cdot\mathring{\mathbf{e}}\right], \tag{7b}$$

where operations beneath an overbar are performed prior to operations above, and where the constant coefficients are

$$\begin{aligned}
&\tilde{\omega}_1 = \frac{4}{3}\left(\frac{7}{2} - s\right), \quad \tilde{\omega}_2 = 2, \quad \tilde{\omega}_3 = 3, \quad \tilde{\omega}_4 = 0, \quad \tilde{\omega}_5 = 3s, \quad \tilde{\omega}_6 = 8, \\
&\theta_1 = \frac{15}{4}\left(\frac{7}{2} - s\right), \quad \theta_2 = \frac{45}{8}, \quad \theta_3 = -3, \quad \theta_4 = 3, \quad \theta_5 = \frac{35}{4} + s.
\end{aligned} \tag{8}$$

The expressions in (7a), (7b) containing the convective derivative, D, are often substituted by approximations derived from the Euler equations, viz.:

$$D\nabla\mathbf{v} = \nabla\left(\mathbf{F} - \frac{\nabla p}{\rho}\right) - \nabla\mathbf{v}\cdot\nabla\mathbf{v}, \tag{9a}$$

$$D\nabla T = -\left(\gamma - 1\right)\nabla\cdot\left(T\nabla\cdot\mathbf{v}\right) - \nabla\mathbf{v}\cdot\nabla T, \tag{9b}$$

where $\mathbf{F}$ is the body force acting on the gas. These approximations mean that additional time-dependent terms do not appear in the governing equations.

It is well known that the Burnett equations are unstable to small wavelength disturbances [5]. For this reason, various authors have proposed modifications to the original equations, which have added or removed terms to attain fine-grid stability in their solutions for hypersonic flows. Recent work by Xue et al. [11] suggests that these problems are encountered when the Burnett equations are applied to micro flows: solutions can only be obtained on very coarse numerical grids for Kn below about 0.18. However, it will be demonstrated here that, for the same application, a new methodology can be developed which achieves numerically stable Burnett solutions for arbitrary grid resolution and Knudsen number.

3. The numerical stability of the Burnett equations applied to micro Couette flow

Couette flow is a straightforward test for methods of modelling micro flows. It is a simple analogue for applications including hard-disc drive reader heads, micro turbines and gas bearings. A schematic for this shear flow (generated within a micro channel by the parallel motion of one of the solid bounding surfaces) is illustrated in Fig. 1, where the important parameters are the micro channel height, H, and the velocity of the moving wall, V.

For steady, parallel (essentially one-dimensional) flow within the micro channel, the Burnett equations reduce to the set of ordinary differential equations:

$$\frac{\mathrm{d}}{\mathrm{d}y}\left(\mu\frac{\mathrm{d}u}{\mathrm{d}y}\right) = 0, \tag{10a}$$

$$\frac{\mathrm{d}}{\mathrm{d}y}\left(\mu u\frac{\mathrm{d}u}{\mathrm{d}y} + \kappa\frac{\mathrm{d}T}{\mathrm{d}y}\right) = 0, \tag{10b}$$

$$\frac{\mathrm{d}}{\mathrm{d}y}\left(p + \Pi_{22}^{(2)}\right) = 0, \tag{10c}$$

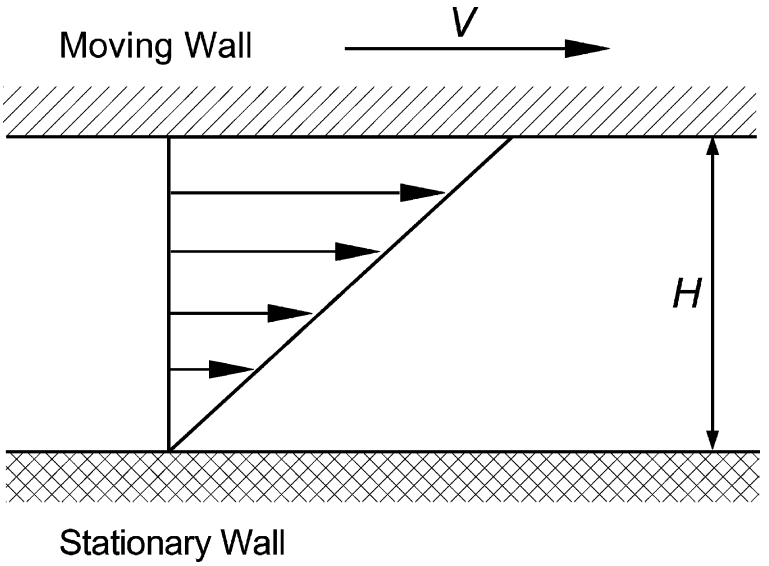

Fig. 1. A schematic of the micro Couette flow under investigation.

where y is the coordinate perpendicular to the flow, u is the streamwise velocity and $\Pi_{ij}^{(2)}$ is the second-order contribution to the stress tensor

$$\Pi_{22}^{(2)} = \frac{\mu^2}{p}\left[\alpha_1\left(\frac{\mathrm{d}u}{\mathrm{d}y}\right)^2 + \alpha_2 R\frac{\mathrm{d}^2T}{\mathrm{d}y^2} + \alpha_3\frac{RT}{\rho}\frac{\mathrm{d}^2\rho}{\mathrm{d}y^2} + \alpha_4\frac{RT}{\rho^2}\left(\frac{\mathrm{d}\rho}{\mathrm{d}y}\right)^2 + \alpha_5\frac{R}{\rho}\frac{\mathrm{d}\rho}{\mathrm{d}y}\frac{\mathrm{d}T}{\mathrm{d}y} + \alpha_6\frac{R}{T}\left(\frac{\mathrm{d}T}{\mathrm{d}y}\right)^2\right], \tag{11}$$

where $\alpha_1 = -(2/3)\tilde{\omega}_2 + (1/12)\tilde{\omega}_6$, $\alpha_2 = -(2/3)\tilde{\omega}_2 + (2/3)\tilde{\omega}_3$, $\alpha_3 = -(2/3)\tilde{\omega}_2$, $\alpha_4 = (2/3)\tilde{\omega}_2$, $\alpha_5 = -(2/3)\tilde{\omega}_2 + (2/3)\tilde{\omega}_4$, and $\alpha_6 = (2/3)\tilde{\omega}_4 + (2/3)\tilde{\omega}_5$. For convenience, flow variables and properties will be non-dimensionalised as follows:

$$\hat{u} = \frac{u}{c_1}, \quad \hat{p} = \frac{p}{p_1}, \quad \hat{T} = \frac{c_p T}{c_1^2}, \quad \hat{\rho} = \frac{\rho c_1^2}{p_1}, \quad \hat{y} = \frac{p_1 y}{\mu_1 c_1}, \quad \hat{\mu} = \frac{\mu}{\mu_1}, \quad \hat{\kappa} = \frac{\kappa}{\mu_1 c_p}, \quad \hat{c}_\mathrm{v} = \frac{c_\mathrm{v}}{c_p},$$
$$\hat{R} = \frac{R}{c_p}, \tag{12}$$

where the subscript 1 denotes a gas property evaluated at the stationary wall of the micro channel. Eqs. (10a), (10b), (10c) can then be written in the form:

$$\frac{\mathrm{d}\hat{T}}{\mathrm{d}\hat{y}}\frac{\mathrm{d}\hat{u}}{\mathrm{d}\hat{y}} + \hat{T}\frac{\mathrm{d}^2\hat{u}}{\mathrm{d}\hat{y}^2} = 0, \tag{13a}$$

$$\frac{2}{3}\hat{T}\left(\frac{\mathrm{d}\hat{u}}{\mathrm{d}\hat{y}}\right)^2 + \left(\frac{\mathrm{d}\hat{T}}{\mathrm{d}\hat{y}}\right)^2 + \hat{T}\frac{\mathrm{d}^2\hat{T}}{\mathrm{d}\hat{y}^2} = 0, \tag{13b}$$

$$\frac{2}{5}\hat{T}\frac{\mathrm{d}\hat{\rho}}{\mathrm{d}\hat{y}} + \frac{2}{5}\hat{\rho}\frac{\mathrm{d}\hat{T}}{\mathrm{d}\hat{y}} + \frac{\mathrm{d}\hat{\Pi}_{22}^{(2)}}{\mathrm{d}\hat{y}} = 0. \tag{13c}$$

On inspection of Eqs. (13a)–(13c) it can be seen that the density features only in Eq. (13c). This allows the velocity and temperature to be solved independently, using only Eqs. (13a) and (13b) and the density

calculated subsequently using Eq. (13c). Both stages of this overall solution strategy will now be considered for stability.

To examine how well-conditioned (and consequently stable) the solution to Eqs. (13a) and (13b) is, velocity and temperature perturbations around a known, assumed solution are considered. Absolute stability or instability cannot be precisely attributed to this analysis, but if the perturbations demonstrate dominant oscillatory (complex eigenvalues) behaviour, it is likely that a numerical solution will be unattainable. The perturbed temperature and velocity solutions can be expressed in the form

$$\hat{u} = u_i + u' \exp\left\{\beta\hat{y}\right\}, \quad \hat{T} = T_i + T' \exp\left\{\beta\hat{y}\right\}, \tag{14}$$

where primed symbols express the perturbation magnitude, β the perturbation growth, and u_i and T_i are the classical, constant-viscosity non-slip Couette flow solutions. Although the constant-viscosity Couette flow profiles are not an exact solution to Eqs. (13a) and (13b), they provide an adequate approximation for the purposes of this analysis

$$u_i = Kn\,M\hat{y}, \quad T_i = \frac{3}{2} + \frac{Kn\,M^2\hat{y}}{3}\left(1 - Kn\hat{y}\right), \tag{15}$$

where the Mach number of the moving wall, M, and Knudsen number, Kn, are defined as

$$M = \frac{V}{c_1}, \quad Kn = \frac{\mu c_1}{pH} \simeq \frac{\lambda}{H}. \tag{16}$$

The constant-viscosity solution and perturbation (Eq. (14)) can now be substituted into Eqs. (13a) and (13b). After linearisation this gives the simultaneous set:

$$\left(\frac{\mathrm{d}T_i}{\mathrm{d}\hat{y}} + T_i\beta\right)\hat{u} + Kn\,M\hat{T} = 0, \tag{17a}$$

$$\left(6\frac{\mathrm{d}T_i}{\mathrm{d}\hat{y}} + 3T_i\beta\right)\hat{T} + 4T_i Kn\,M\hat{u} = 0. \tag{17b}$$

These expressions are combined to give the characteristic equation

$$\beta^2 + 3\left(\frac{1}{T_i}\frac{\mathrm{d}T_i}{\mathrm{d}\hat{y}}\right)\beta + 2\left(\frac{1}{T_i}\frac{\mathrm{d}T_i}{\mathrm{d}\hat{y}}\right)^2 - \frac{4Kn^2M^2}{3T_i} = 0, \tag{18}$$

the roots of which are real for every point across the channel and for any Mach or Knudsen number, since

$$\left(\frac{1}{T_i}\frac{\mathrm{d}T_i}{\mathrm{d}\hat{y}}\right)^2 + \frac{16Kn^2M^2}{3T_i} \geqslant 0. \tag{19}$$

This means that no oscillatory perturbations away from the known solution are present. This strongly suggests that the solution of Eqs. (13a) and (13b) will be stable.

To demonstrate the stability of this stage of the solution, a simple implicit centred-difference scheme has been used to solve Eqs. (13a) and (13b), using non-slip wall boundary conditions for $Kn = 1$ and $M = 3$. Convergence was assumed when

$$\max\left[\frac{\hat{u} - \hat{u}_{\mathrm{old}}}{c_1 M}, \quad \frac{\hat{T} - \hat{T}_{\mathrm{old}}}{T_1}\right] \leqslant 10^{-12}, \tag{20}$$

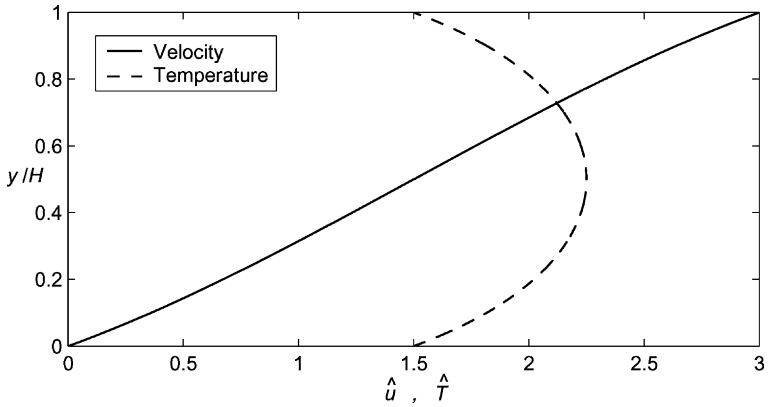

Fig. 2. Calculated velocity and temperature distributions across the channel in micro Couette flow for $Kn = 1$, $M = 3$.

where the subscript old refers to values from a previous iteration. In these simulations no numerical stability problems were encountered, even though over a thousand grid points were used across the channel. The velocity and temperature profiles are shown in Fig. 2.

The second stage of the solution is the calculation of the density distribution. This involves the evaluation of terms generated from the Burnett approximation. Since there are third-order spatial terms in Eq. (13c), an extra boundary condition is required. Here, as in the approach adopted by Xue et al. [11], the equation for density is integrated to reduce the order:

$$\rho RT + \Pi_{22}^{(2)} = A, \tag{21}$$

where A is an unknown integration constant. The extra information required to find a unique solution to Eq. (21) is obtained by observing that the Burnett equations are equivalent to the Navier–Stokes equations as Kn tends to zero, therefore

$$\left.\begin{array}{l} p = p_1 \\ \Pi_{22}^{(2)} = 0 \end{array}\right\} \quad \text{as } Kn \to 0. \tag{22}$$

If it is assumed that A is independent of Kn, this can be used in place of an additional boundary condition for Eq. (21), to give

$$\rho RT + \Pi_{22}^{(2)} = p_1. \tag{23}$$

The stability of solutions to Eq. (23) are investigated (as before) by considering perturbations from the constant-viscosity solution (Eq. (15))

$$\hat{\rho} = \frac{5}{2T_i} + \bar{\rho}\exp\{\beta\hat{y}\}. \tag{24}$$

The characteristic equation for density perturbations, after the linearisation of Eq. (23), is then

$$8T_i\beta^2 + 24\frac{\mathrm{d}T_i}{\mathrm{d}\hat{y}}\beta - \frac{27}{5}\rho_i^2 = 0. \tag{25}$$

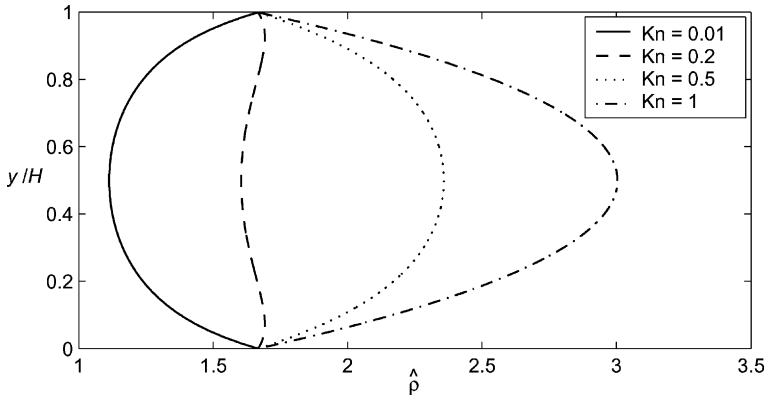

Fig. 3. Calculated density distributions across the channel in micro Couette flow for $M = 3$, $Kn = 0.01$, 0.1, 0.5 and 1.

The roots of the characteristic equation (25) will always be real, irrespective of the values for Kn and M, since

$$10\left(\frac{\mathrm{d}T_i}{\mathrm{d}\hat{y}}\right)^2 + 3\rho_i^2 T_i \geqslant 0. \tag{26}$$

Consequently, a stable solution, uncorrupted by oscillations, should be obtainable. To demonstrate this point, Eq. (13c) has been solved numerically using over a thousand grid points – Fig. 3 shows the density distributions for varying Kn at $M = 3$. No stability problems were encountered.

4. Slip boundary conditions

The analysis so far has shown nothing to indicate that the Burnett equations are unstable when applied to micro Couette flow. However, Xue et al. [11] encountered serious stability problems that prevented them from obtaining micro Couette solutions for $Kn \gtrsim 0.18$ (for $M = 3$). The reason for this problem, as will be shown here, is boundary condition instability.

In general, non-slip boundary conditions are unrealistic for continuum transition flows as there are not enough collisions near the wall to equilibrate the flow field. For this reason *slip* conditions should be prescribed at the wall. The classical boundary conditions of this type are the Maxwell/Smoluchowski first-order slip conditions:

$$u_\mathrm{s} - u_\mathrm{w} = \frac{2-\sigma_u}{\sigma_u}\lambda\left.\frac{\mathrm{d}u}{\mathrm{d}y}\right|_\mathrm{w}, \tag{27a}$$

$$T_\mathrm{s} - T_\mathrm{w} = \frac{2-\sigma_T}{\sigma_T}\frac{2\gamma}{\mathrm{Pr}\,(\gamma+1)}\lambda\left.\frac{\mathrm{d}T}{\mathrm{d}y}\right|_\mathrm{w}, \tag{27b}$$

where the subscripts s and w denote slip and wall values, and σ_u, σ_T are, respectively, the tangential-momentum and thermal accommodation coefficients. The thermal creep term sometimes included in Eqs. (27a) is neglected here, since the Reynolds number for this application is relatively large. If the incident tangential momentum and energy flux is equal to that reflected ($\sigma_u = 0, \sigma_T = 0$) the non-dimensionalised form of conditions (27a), (27b) are:

$$\hat{u}_s = \hat{u}_w + \sqrt{\frac{8}{27}\hat{T}_s^3}\left.\frac{d\hat{u}}{d\hat{y}}\right|_w, \tag{28a}$$

$$\hat{T}_s = \frac{3}{2} + \sqrt{\frac{25}{24}\hat{T}_s^3}\left.\frac{d\hat{T}}{d\hat{y}}\right|_w. \tag{28b}$$

Note that the velocity slip and temperature jump conditions are independent of density – this maintains the decoupled nature of the density, allowing it to be calculated secondarily.

The problems associated with using these boundary conditions are revealed by examining the solutions to Eqs. (28a), (28b) in the first iteration of a calculation. If it is assumed that the viscosity is constant, evaluation of the momentum equation (10a) at the stationary wall gives

$$\left.\frac{d\hat{u}}{d\hat{y}}\right|_w = Kn\,(M - 2\hat{u}_s). \tag{29}$$

When this is combined with Eq. (28a), expressions for the velocity slip and velocity gradient at the stationary wall are obtained:

$$\hat{u}_s = \frac{Kn\,M\sqrt{8\hat{T}_s^3}}{\sqrt{27} + 2Kn\sqrt{8\hat{T}_s^3}}, \tag{30a}$$

$$\left.\frac{d\hat{u}}{d\hat{y}}\right|_w = \frac{\sqrt{27}Kn\,M}{\sqrt{27} + 2Kn\sqrt{8\hat{T}_s^3}}. \tag{30b}$$

Since this is a first iteration solution ($T_s = T_1$) the expression for the velocity gradient is simply

$$\left.\frac{d\hat{u}}{d\hat{y}}\right|_w = \frac{Kn\,M}{1 + 2Kn}. \tag{31}$$

Now, by evaluating the energy equation (10b) at the stationary wall (again, with viscosity assumed constant) the following relationship between the velocity and temperature gradient is found

$$\left.\frac{d\hat{T}}{d\hat{y}}\right|_w = \frac{1}{3Kn}\left.\frac{d\hat{u}}{d\hat{y}}\right|_w^2. \tag{32}$$

Finally, by combining Eqs. (28b), (31) and (32), a cubic expression for the temperature jump boundary condition can be obtained

$$\frac{25Kn^2M^4}{54(1 + 2Kn)^4}\hat{T}_s^3 - 4\hat{T}_s^2 + 12\hat{T}_s - 9 = 0. \tag{33}$$

Solutions to this equation are physically meaningful if they are real (i.e., have no complex components) and satisfy the condition $\hat{T}_s \geqslant 3/2$ (from Eq. (28b), given that for Couette flow $(d\hat{T}/d\hat{y})|_w > 0$). Fig. 4 shows the roots of Eq. (33) for $M = 3$ at varying Kn values – physical solutions only occur for $Kn \leqslant 0.2$. Note also that in approaching this Kn value there is likely to be solution difficulty because of the competing physical roots; at these points it is not clear which of the roots is more 'physical', and this ambiguity prevents a straightforward numerical solution. This is the reason why Xue et al. [11] reported an inability to produce micro Couette simulations beyond about $Kn = 0.18$, in line with the predictions of this analysis.

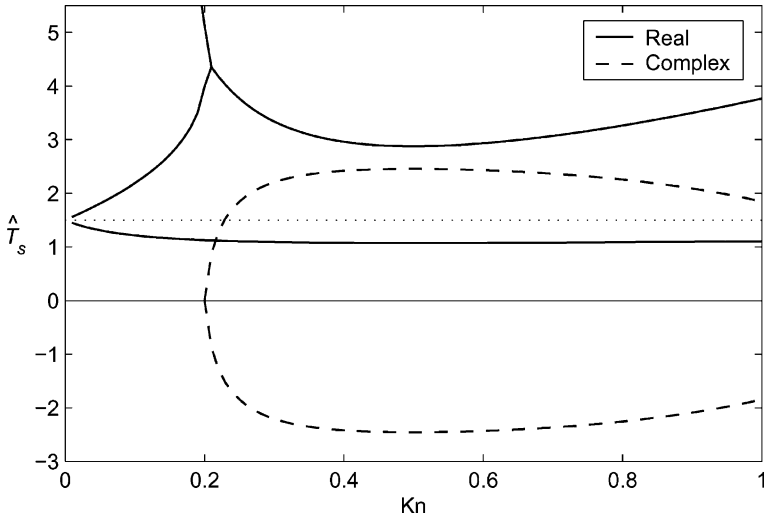

Fig. 4. Roots of cubic equation for temperature-jump boundary condition for varying Kn. The dotted line indicates $\hat{T}_s = 3/2$, under which real roots are non-physical.

To eliminate this problem, the numerical scheme for solving the temperature boundary condition should be semi-implicit rather than fully implicit. In other words, part of the solution for the slip condition (28b) should be based on values of $\hat{T}_s$ from a previous iteration ($\hat{T}_{old}$). If the mean free path is taken as $\hat{\lambda} = \hat{T}_s\sqrt{8\hat{T}_{old}/27}$, instead of $\hat{\lambda} = \sqrt{8\hat{T}_s^3/27}$, an alternative cubic expression for the temperature jump can be obtained:

$$\left(\frac{32Kn\,\hat{T}_{old}}{27}\right)\widehat{T}_s{}^3 - \left(\frac{16Kn\,\hat{T}_{old}}{9} - 4\sqrt{\frac{8\hat{T}_{old}}{27}}\right)\widehat{T}_s{}^2 - \left(\sqrt{\frac{32\hat{T}_{old}}{3}} + \frac{M^2}{3}\sqrt{\frac{25\hat{T}_{old}}{24}} - \frac{1}{Kn}\right)\widehat{T}_s - \frac{3}{2Kn} = 0. \quad (34)$$

The roots of Eq. (34) for $M = 3$, $T_{old} = T_1$, and varying Kn are shown in Fig. 5. There is exactly one positive real root for every Knudsen number on the scale, and since negative temperatures are non-physical, a numerical solution of the full equations will always tend to this, provided appropriate initial conditions are chosen. Normally, the temperature jump condition would be solved implicitly as part of the energy equation. The improvement in stability is owed to the relaxation that is indirectly applied to the boundary condition as a result of the semi-implicitness.

An alternative approach is to solve the slip and jump conditions explicitly, i.e., independently of the momentum and energy equations. In this way relaxation can be applied and controlled exclusively to the boundary conditions (note, this is not the same as applying relaxation to the flow variables). Fig. 6 demonstrates the stabilising influence that boundary condition relaxation has on the full equations, where the relaxation factor, R_f, is used to calculate the boundary condition for the new iteration as follows:

$$\hat{T}_{new} = \hat{T}_{old} + R_f\left(\hat{T}_s - \hat{T}_{old}\right). \quad (35)$$

As predicted by Fig. 4, solutions with Kn values much greater than 0.2 cannot be obtained when the boundary conditions are treated normally (i.e. $R_f = 1.0$). However, a relaxation value of 0.2 is enough to achieve unique solutions for Knudsen numbers up to and above $Kn = 1$.

Numerical convergence can be speeded up considerably by choosing a more suitable initial distribution for velocity and temperature. In the previous examples, an initial constant-viscosity, non-slip solution to

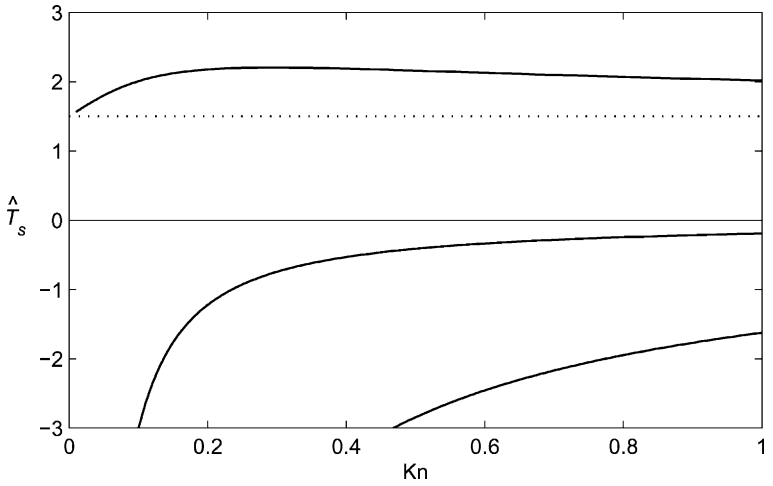

Fig. 5. Roots of cubic equation for semi-implicit temperature-jump boundary condition against Kn. The dotted line indicates $\hat{T}_s = 3/2$, under which real roots are non-physical. In this case, all roots are real.

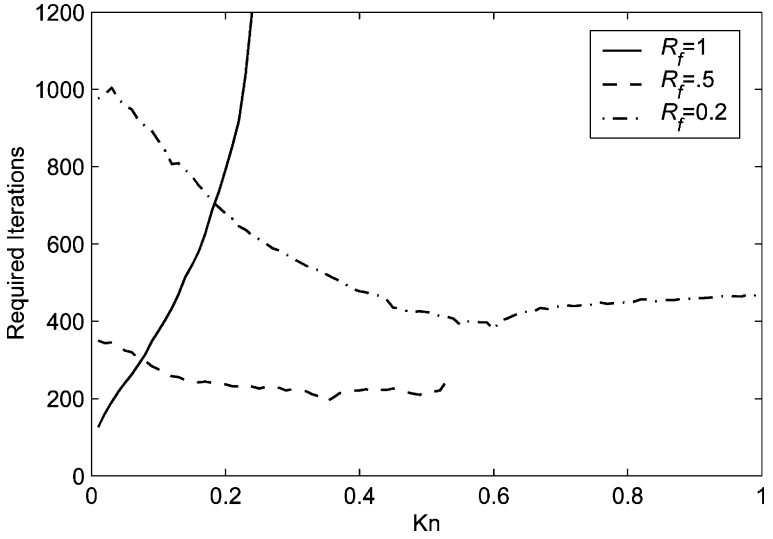

Fig. 6. Iterations required for convergence, against Kn, for different levels of boundary condition relaxation (R_f).

Eqs. (10a), (10b), (10c) was used. However, if Eq. (34) is solved iteratively, slip values can be obtained and used to construct a constant-viscosity *slip* solution – this provides a much better initial guess. In Figs. 7 and 8, the velocity slip and temperature jump values predicted by Eqs. (30a) and (34) are compared to those calculated by the full model using boundary condition relaxation. The prediction of the constant-viscosity/slip solution is remarkably close to the final solution.

From the analysis of this section it can be concluded that the Burnett equations are not an inherently unstable approximation when used to model micro Couette flow. The instabilities reported by Xue et al. [11] for micro Couette flow were a result of the slip boundary conditions used and not the Burnett equations themselves.

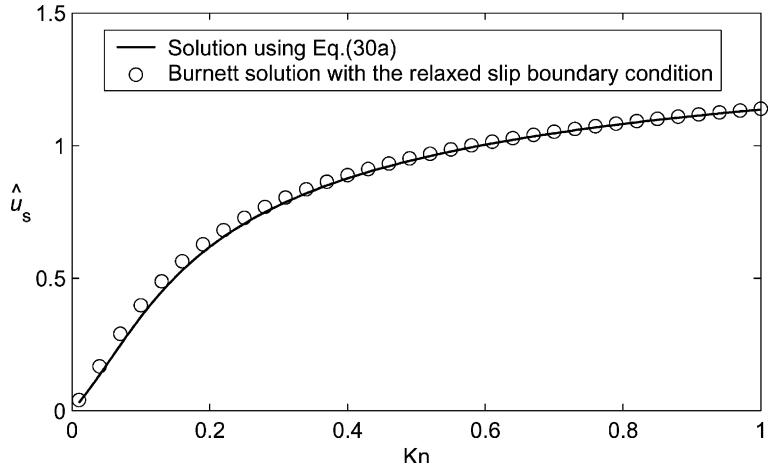

Fig. 7. Comparison of the velocity slip ($\hat{u}_s$) calculated by a full simulation (○) and the constant-viscosity/slip analysis (–).

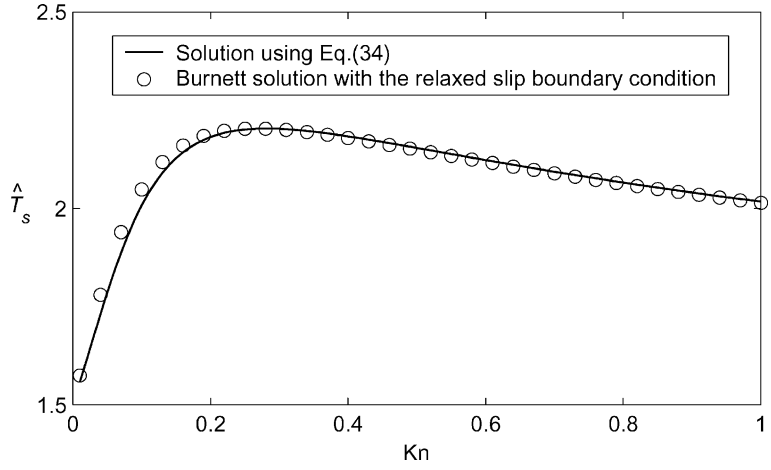

Fig. 8. Comparison of the temperature-jump condition ($\hat{T}_s$) calculated by a full simulation (○) and the constant-viscosity/slip analysis (–).

5. Micro Couette results

There is a shortage of reliable experimental data in microfluidics, so DSMC (direct simulation Monte Carlo) models are often used as a convenient experimental analogue (especially for simple flow geometries). In this section, the Burnett equations are solved for micro Couette flow by the method described in Sections 3 and 4, and compared with the DSMC results of Nanbu [8].

For these simulations, a hundred finite-difference points have been used with a convergence criteria described by Eq. (20). As discussed in Section 4, a first-order slip condition (Maxwell/Smoluchowski) can be used to resolve non-equilibrium flow effects at the wall. The utility of a second-order approximation can also be investigated [6]:

$$u_s - u_w = \frac{2-\sigma_u}{\sigma_u}\left(\lambda \left.\frac{du}{dy}\right|_w + \frac{\lambda^2}{2}\left.\frac{d^2u}{dy^2}\right|_w\right), \tag{36a}$$

$$T_s - T_w = \frac{2-\sigma_T}{\sigma_T}\frac{2\gamma}{Pr(\gamma+1)}\left(\lambda \left.\frac{dT}{dy}\right|_w + \frac{\lambda^2}{2}\left.\frac{d^2T}{dy^2}\right|_w\right). \tag{36b}$$

Fig. 9 shows the variation of wall heat flux with Kn (at $M = 3$) compared to results obtained from a DSMC simulation [8]. Results from using three different wall-boundary approximations are shown: the non-slip condition, the first-order Maxwell/Smoluchowski (M/S) slip condition, and the second-order approximation (36a), (36b). The non-slip condition provides a good prediction for wall heat flux for Kn up to about 0.04, after which the results begin to diverge rapidly from the DSMC data – it is clear that non-slip conditions are not adequate for modelling micro Couette flows across the full range of Kn. The first-order slip conditions, however, continue to provide close agreement with DSMC up until around $Kn = 0.1$, though only qualitative agreeement can be observed at $Kn = 1$. In any case, as the Burnett equations arise from a Kn-series solution to the fundamental gas kinetic equation which is assumed to converge, Burnett solutions as $Kn \to 1$ cannot be expected to produce highly accurate results as they are being applied at the limit of their validity.

Intuitively, the first-order conditions should provide a poorer approximation than the second-order slip conditions. However, the fact that the opposite is shown to be the case in Fig. 9 may reflect a fundamental inaccuracy in the second-order M/S-type slip conditions at high Kn. This result could warrant future investigation into alternative slip boundary conditions, such as those recently proposed by Myong [7]. These boundary conditions circumvent the difficulty in assigning the accommodation coefficients used in Eqs. (27a), (27b) and (36a), (36b), by modelling the gas-surface molecular interaction process as a chemical adsorption.

Fig. 10 shows a comparison of the present results with DSMC simulations for the wall shear stress at $M = 3$ for varying Kn. A similar advantage in using slip conditions over non-slip conditions is demonstrated, though the improvement when using a first-order instead of a second-order approximation is less

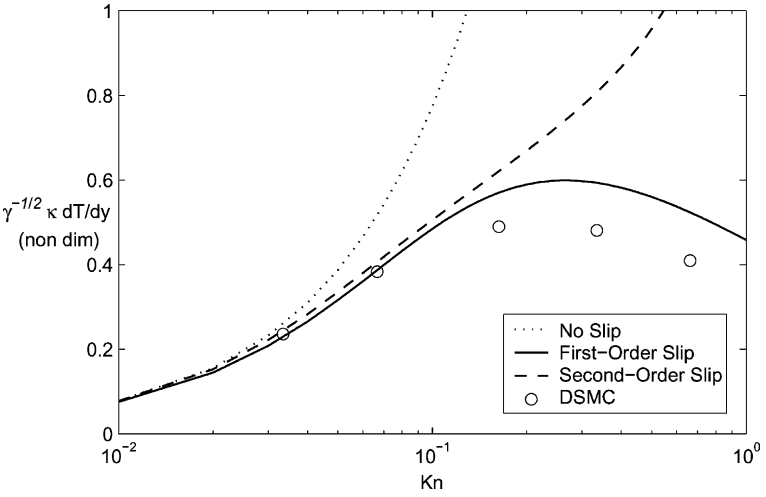

Fig. 9. Variation of non-dimensional wall heat flux with Kn. Comparison of DSMC results with Burnett solutions using non-slip and various slip boundary conditions ($M = 3$).

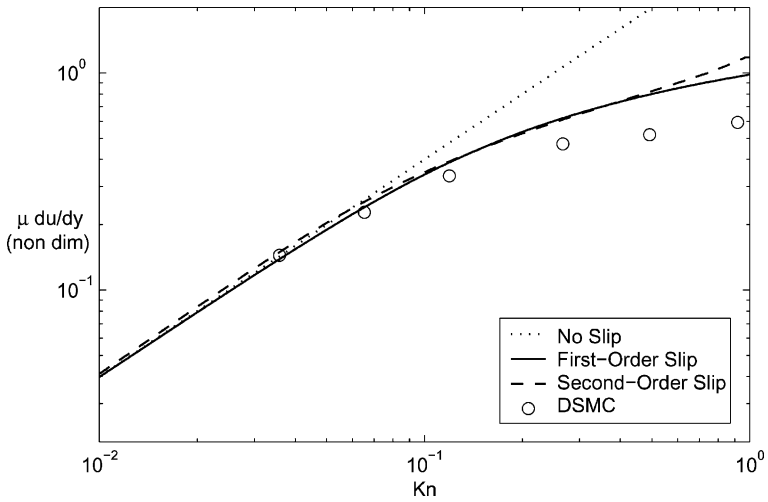

Fig. 10. Variation of non-dimensional wall shear stress with Kn. Comparison of DSMC results with Burnett solutions using non-slip and various slip boundary conditions ($M = 3$).

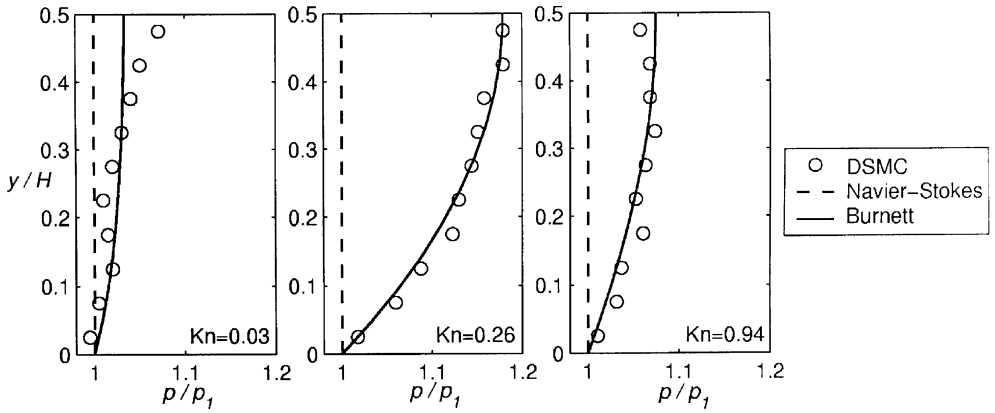

Fig. 11. Distribution of non-dimensional pressure across the micro channel for $M = 3$ (half-channel, but symmetry can be assumed), for various Kn.

pronounced. This is because the second derivative of the velocity distribution is smaller, relative to the first derivative, than the equivalent derivatives in the temperature distribution. The velocity slip is therefore less affected by a second-order approximation than the temperature, and consequently so is the wall shear stress.

A final confirmation of the general utility of the Burnett equations for this application is demonstrated by calculations of the pressure distribution across the micro channel as shown in Fig. 11. Here, the DSMC data of Nanbu [8] are compared with the Burnett solutions and the classical Navier–Stokes solutions using first-order slip conditions. What is most noticeable is that the Navier–Stokes solution predicts no pressure variation across the micro channel. The Burnett equations, on the other hand, agree with the DSMC predictions for all Kn values considered.

6. Conclusions

It has been demonstrated that for steady monatomic gas flows in simple microfluidic geometries the Burnett equations form a numerically stable set of governing equations. Previous problems encountered when solving the Burnett equations in these geometries are a result of an incorrect application of the boundary conditions, and not due to any intrinsic and fundamental instability present in the model equations. By treating the slip boundary conditions either semi-implicitly, or using a relaxation method, solutions can be obtained over the full range of Kn (on arbitrarily fine numerical grids).

Burnett solutions using relaxed first-order slip conditions agree very well with direct simulations up to the expected limit of validity of the equations, and are orders of magnitude quicker to obtain than the corresponding DSMC data. To quicken convergence further, a constant-viscosity/slip solution can be constructed to predict the first-order slip conditions prior to the solution of the full equations – this provides a better initial guess for the first iteration. The poorer agreement with DSMC data when using second-order slip conditions may indicate a fundamental problem with higher-order M/S conditions and requires further investigation.

The Burnett equations have, in general, been shown to be an excellent model for simple gas flows in microfluidic applications. Further work could usefully include: investigating Burnett solutions of Poiseuille flow in a micro channel; extending the governing equations to model air flows; applying the Burnett equations to two- and three-dimensional micro geometries.

Acknowledgements

The authors are grateful to H. Xue for his assistance and consultations, L.C. Woods for his helpful comments on an earlier draft of this paper, and the Leverhulme Trust for supporting the project.

References

[1] R.K. Agarwal, K.Y. Yun, R. Balakrishnan, Beyond Navier–Stokes: Burnett equations for flows in the continuum-transition regime, Phys. Fluids 13 (10) (2001) 3061.
[2] S. Chapman, T.G. Cowling, The Mathematical Theory of Non-Uniform Gases, third ed., Cambridge University Press, Cambridge, 1970.
[3] M. Gad-el-Hak, The fluid mechanics of microdevices, J. Fluid Eng. T. ASME 121 (1) (1999) 5.
[4] C.M. Ho, Y.C. Tai, Micro-electro-mechanical-systems and fluid flows, Ann. Rev. Fluid Mech. 30 (1998) 579.
[5] S. Jin, M. Slemrod, Regularization of the Burnett equations via relaxation, J. Stat. Phys. 103 (2001) 1009.
[6] G.E. Karniadakis, A. Beskok, Micro Flows: Fundamentals and Simulation, Springer, Berlin, 2002.
[7] R.S. Myong, A computational method for Eu's generalized hydrodynamic equations of rarefied and microscale gasdynamics, J. Comput. Phys. 168 (2001) 47.
[8] K. Nanbu, Analysis of the Couette flow by means of the new direct-simulation method, J. Phys. Soc. Jpn. 52 (1983) 5.
[9] J.M. Reese, L.C. Woods, F.J.P. Thivet, S.M. Candel, A second-order description of shock structure, J. Comput. Phys. 117 (1995) 240.
[10] L.C. Woods, An Introduction to the Kinetic Theory of Gases and Magnetoplasmas, Oxford University Press, Oxford, 1993.
[11] H. Xue, H.M. Ji, C. Shu, Analysis of micro-Couette flow using the Burnett equations, Int. J. Heat Mass Transfer 44 (21) (2001) 4139.
[12] X.L. Zhong, R.W. MacCormack, D.R. Chapman, Stabilization of the Burnett equations and application to hypersonic flows, AIAA J. 31 (6) (1993) 1036.